JACS
JOURNAL OF THE AMERICAN CHEMICAL SOCIETY
Article
pubs.acs.org/JACS

Two-Dimensional π-Expanded Quinoidal Terthiophenes Terminated with Dicyanomethylenes as n-Type Semiconductors for High-Performance Organic Thin-Film Transistors

Cheng Zhang,[†,‡] Yaping Zang,[†,‡] Eliot Gann,[§,∥] Christopher R. McNeill,[∥] Xiaozhang Zhu,*[,†] Chong-an Di,*[,†] and Daoben Zhu[†]

[†]Beijing National Laboratory for Molecular Sciences, CAS Key Laboratory of Organic Solids, Institute of Chemistry, Chinese Academy of Sciences, Beijing 100190, P. R. China

[‡]University of Chinese Academy of Sciences, Beijing 100049, P. R. China

[§]Australian Synchrotron, 800 Blackburn Road, Clayton, Victoria 3168, Australia

[∥]Department of Materials Engineering, Monash University, Clayton, Victoria 3800, Australia

Supporting Information

ABSTRACT: Quinoidal oligothiophenes (**QOT**), as classical n-type semiconductors, have been well-known for a long time but with non-optimal semiconducting properties. We report here the design and selective synthesis of new two-dimensional (2D) π-expanded quinoidal terthiophenes, **2DQTTs**, with proximal (**2DQTT-i**) and distal (**2DQTT-o**) regiochemistry for high-performance n-channel organic thin-film transistors (n-OTFTs) featuring high electron mobility, solution processability, and ambient stability. The elegant combination of thieno[3,4-*b*]thiophene [TT, donor (D)] and 5-alkyl-4*H*-thieno[3,4-*c*]pyrrole-4,6(5*H*)-dione [TPD, acceptor (A)] units with relatively large π-surface endows these **2DQTTs** with distinctive 2D structural characteristics and flat configuration stabilized by weak intramolecular S−O/S weak interactions. Furthermore, the A−D−A−D−A electronic structure maintains an adequately low LUMO energy level. These **2DQTTs** are shown to exhibit outstanding semiconducting properties with electron mobilities of up to 3.0 $cm^2\ V^{-1}\ s^{-1}$ and on/off ratios of up to 10^6 (**2DQTT-o**) in ambient- and solution-processed OTFTs. Investigations on thin-film morphology reveal that the microstructure of **2DQTTs** is highly dependent on the orientation of the fused thiophene subunits, leading to differences in electron mobilities of 1 order of magnitude. X-ray diffraction studies in particular reveal increased crystallinity, crystalline coherence, and orientational order in **2DQTT-o** compared to **2DQTT-i**, which accounts for the superior electron transport property of **2DQTT-o**.

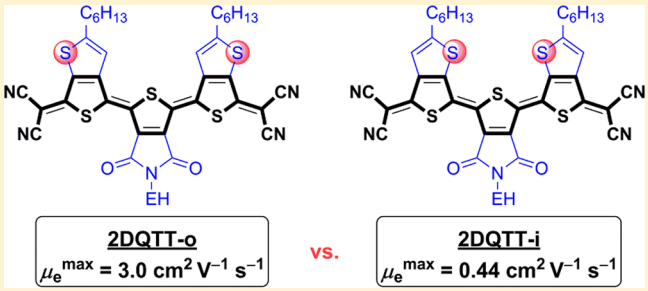

INTRODUCTION

For n-type organic semiconductors,[1] control of the lowest unoccupied molecular orbital (LUMO) energy level is a prerequisite for ambient-stable n-channel organic thin-film transistors (n-OTFTs),[2] which has contributed to the sluggish development of this technology. Among various types of n-type organic semiconductors reported, quinoidal oligothiophenes (**QOTs**)[3] have been recognized as promising n-type semiconductors with appropriate LUMO energy levels (<−3.9 eV vs the vacuum level) derived from the quinoidal molecular structure terminated by two strongly electron-withdrawing dicyanomethylenes. Considerable efforts have been made to develop new **QOTs** for high-performance OTFTs, by means of improving solubility[4] and enhancing intermolecular interactions by utilizing fused thiophene frameworks[5] or incorporating selenophene units.[6] However, despite over 10 years of explorations,[3a] the electron mobilities of **QOTs** are still lower than 1.0 $cm^2\ V^{-1}\ s^{-1}$, the median value of amorphous silicon, which makes them apparently less promising than state-of-the-art rylene diimides.[7]

Compared with perylene dimide (PDIs) derivatives[8] with large polycyclic aromatic hydrocarbon (PAH) cores, linear **QOTs** show a smaller π-surface, which may negatively affect the magnitude of the transfer integral, an important factor for charge transport in organic semiconductors.[9] The mobility bottleneck of **QOTs** might be solved by overcoming the key issue of limited π−π intermolecular stacking related to their linear molecular structure. Thus, we selected thieno[3,4-*b*]thiophene[10] and 5-alkyl-4*H*-thieno[3,4-*c*]pyrrole-4,6(5*H*)-dione[11] units with relatively large π-surfaces for the construction of new 2D π-expanded quinoidal terthiophenes, **2DQTT-i** and **2DQTT-o** (Figure 1). Besides the expanded conjugation surfaces for better intermolecular π−π interaction,[12] the combination of TT

Received: June 26, 2014
Published: October 28, 2014

   dx.doi.org/10.1021/ja510003y | J. Am. Chem. Soc. 2014, 136, 16176−16184

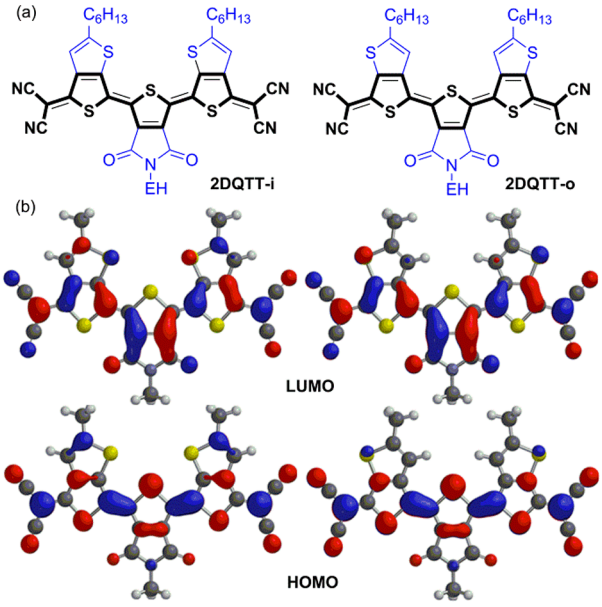

Figure 1. Molecular structures (a), optimized geometry and HOMO/LUMO orbitals of **2DQTT-i** and **2DQTT-o** (b) (EH = 2-ethylhexyl). (Calculations were conducted at the DFT//B3LYP/6-31G* level. Alkyl substituents were replaced by methyl groups to simplify the calculations.)

Scheme 1. Selective Synthesis of Compounds 2DQTT-i, 2DQTT-o, and QTT[a]

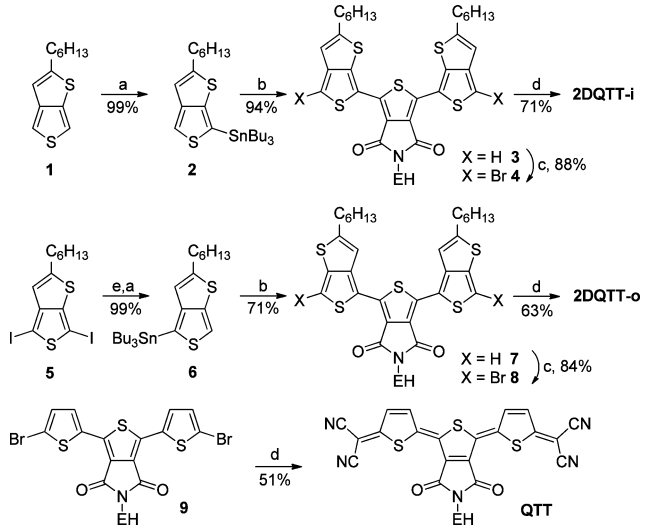

[a]Reagents and conditions: (a) (i) *n*-BuLi, THF, −78 °C; (ii) tributyltin chloride; (b) TPD-2Br, $Pd(PPh_3)_4$, toluene/DMF, 90 °C; (c) NBS, DMF/$CHCl_3$, rt; (d) (i) malonitrile, NaH, $Pd(PPh_3)_4$, 1,4-dioxane, 100 °C; (ii) HCl, DDQ, rt; (e) (i) *n*-BuLi, THF, −78 °C; (ii) H_2O.

and TPD units endows the molecules with additional distinct structural characteristics: (1) The flat configuration can be stabilized by weak intramolecular S−O and/or S (lateral thiophene)−S (central thiophene) interactions;[13] (2) the A−D−A−D−A electronic structure can keep the LUMO levels adequately low; (3) the alkyl substituents of TPD units provide additional opportunities for tuning solubility and thin-film morphology of the semiconducting layer based on **2DQTT**s in OTFTs.[14]

We report herein the design and selective synthesis of new 2D π-expanded quinoidal terthiophenes, **2DQTT-i** and **2DQTT-o** (Figure 1), for high-performance n-type OTFTs featuring high electron mobility, solution processability, and ambient stability. Both compounds showed electron mobilities of over 10^{-1} cm^2 V^{-1} s^{-1}. Intriguingly, we find that the observed electron mobilities are highly dependent on the orientation of two fused TT subunits with a significant difference of 1 order of magnitude. OTFT devices based on **2DQTT-o** gave high electron mobilities of up to 3.0 cm^2 V^{-1} s^{-1} with current on/off ratios from about 10^5 to 10^6, revealing the great potential of **2DQOT** framework for applications in n-type organic semiconductors.

RESULTS AND DISCUSSION

Synthesis of 2DQTTs. The selective synthesis of **2DQTT-i** and **2DQTT-o** is shown in Scheme 1. Interestingly, deprotonation of TT[15] by *n*-butyllithium at −78 °C in THF occurred exclusively at the 6-position and after addition of tributyltin chloride gave tributyl(2-hexylthieno[3,4-*b*]thiophen-6-yl)stannane **2** in 99% yield. The Stille coupling reaction between compound **2** and 1,3-dibromo-5-(2-ethylhexyl)-4*H*-thieno[3,4-*c*]pyrrole-4,6(5*H*)-dione (TPD-2Br) afforded compound **3** in excellent yield of 94%. After bromination of compound **3**, compound **4** was obtained and subjected to Pd-catalyzed coupling with sodium dicyanomethanide followed by DDQ oxidation to give **2DQTT-i** as a brick-red solid in 71% yield. Compound **2** was synthesized through a similar procedure. The key intermediate tributyl(2-hexylthieno[3,4-*b*]-thiophen-4-yl)stannane **6** was obtained from 2-hexyl-4-iodothieno-[3,4-*b*]thiophene, which could be synthesized by the highly selective Li−I exchange reaction between 2-hexyl-4,6-diiodothieno-[3,4-*b*]thiophene **5** and *n*-butyllithium at the 6-position of TT followed by a second Li−I exchange at the 2-position. The selective deprotonation or Li−I exchange reactions at the 6-position of TT might be individually ascribed to the high acidity or Li−S interaction from the adjacent sulfur atoms. The reference quinoidal terthiophene (**QTT**) without fused thiophene units was also synthesized for comparison. **2DQTT-i**, **2DQTT-o**, and **QTT** showed good thermal stability (up to 290, 306, and 357 °C, respectively, at which 5 wt % loss was recorded, see Supporting Information) and ample solubility in $CHCl_3$ (about 15 mg/mL) at room temperature (rt), which guaranteed solution-based fabrication of OTFT devices.

2DQTT-i and **2DQTT-o** were fully characterized by conventional NMR and mass and elemental analysis. The ^1H NMR spectrum of **2DQTT-i** showed a single peak in the aromatic region, δ 7.66 ppm, which can be assigned to β-hydrogens of the two equivalent fused thiophene subunits, and remained unchanged in deuterated chloroform for days, which indicated the absence of an isomerization process.[16] From the theoretical calculation at the B3LYP/6-31G* level (Figure 1b), we found that **2DQTT-i** had a planar molecular structure with short multiple O−S and S−S interactions with distances of 2.898 Å for O−S and 3.204 Å for S−S, which were smaller than the sum of O, S (3.32 Å) and S, S (3.60 Å) van der Waals radii. However, for **2DQTT-o**, we observed two groups of signals in the aromatic region, which suggested the existence of two stereoisomers because of the reduced intramolecular interactions. The main isomer with a single peak at 7.28 ppm was assigned to the molecular structure with an *E*,*E*-configuration in the terthienoquinoidal core as shown in Figure 1a. The other isomer had two signals at 7.31 and 7.66 ppm, which we assigned to an *E*,*Z*-configuration in the terthienoquinoidal core.

dx.doi.org/10.1021/ja510003y | J. Am. Chem. Soc. 2014, 136, 16176−16184

The ratio of two stereoisomers was determined to be 86:14 based on the integration of the related hydrogen signals. Because the isomer ratios did not change after recrystallizing the products three times, we deduced that the isomers existed in the solution as a thermodynamic equilibrium. During the growth of single crystals, we found that only very thin flake crystals could be obtained for **2DQTT-i**, which were proved to be twin crystals and were not suitable for X-ray structural analysis. After numerous attempts, single crystals of **2DQTT-o** were finally obtained that were suitable for X-ray analysis from mixed dichloromethane/ethyl acetate solvent. Although the single crystal of **2DQTT-o** was measured at the low temperature, 113 K, to prevent unfavorable effects from the molecular vibration, we could not obtain clear diffraction points of the carbon atoms in the alkyl chains, and instead, dispersive ones were observed. To solve this problem, we limited the location of carbon atoms of the alkyl chains manually by the isotropic method, which resulted in a relatively large *R* value (0.17). Fortunately, the diffraction from the conjugated backbone could be easily confirmed and treated by the anisotropy method, and we did not find any errors from the conjugated backbone. The *E*,*E*-configuration of **2DQTT-o** is shown in Figure 2. **2DQTT-o** is almost planar with a small torsional

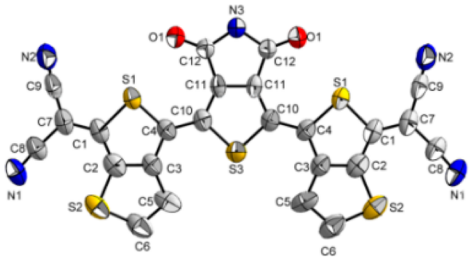

Figure 2. Molecular structures of **2DQTT-o** with 50% probability ellipsoids. (The alkyl chains are omitted for clarity.)

angle of 5.27°. The short distance S−O contact (2.834 Å), which can be clearly observed, is very close to the calculated value (2.850 Å) obtained from the theoretically optimized structure and contributes to the planar molecular structure.[13] Combining the suitable side chains attached on the conjugated backbone, *n*-hexyl groups at the 2-position of TTs and 2-ethylhexyl groups on the TPD, **2DQTT-o** shows a packing mode of "brick-layer" arrangement (Figure S5−S8) with impact slipped $\pi-\pi$ intermolecular interactions of 3.441 Å, which is different from the herringbone packing of the classical linear quinoidal terthiophenes.[3a]

Absorption and Electrochemical Properties of 2DQTTs. The physical properties of **2DQTT-i** and **2DQTT-o** in diluted dichloromethane solution and thin films were investigated. Both compounds show intense near-infrared absorptions at 774 nm (**2DQTT-i**) and 750 nm (**2DQTT-o**) as shown in Figure 3. Compared with that in solution, the maximum absorption of **2DQTT-o** in film was significantly bathochromically shifted to 952 nm by 202 nm, which suggests the existence of a *J*-aggregation, an encouraging indication for favorable electron transfer in thin-film devices.[17] By contrast, the absorption band of **2DQTT-i** in thin film simply became broadened, but still with a comparable absorption maximum at 782 nm. Thus, the aggregation patterns of **2DQTT-i** and **2DQTT-o** in thin films should be different, which accordingly could result in differing OTFT performance. Because of the quinoidal

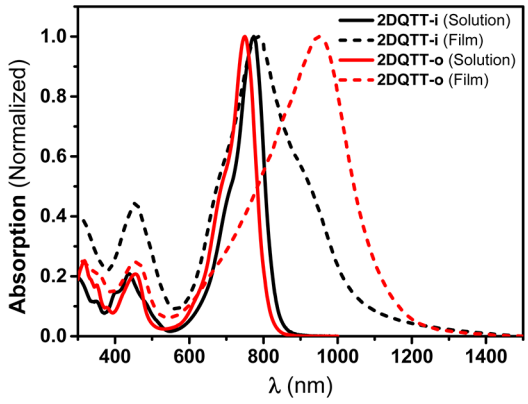

Figure 3. Absorption spectra of **2DQTT-i** (black) and **2DQTT-o** (red) in dichloromethane (solid lines) and thin-film states (dashed lines).

backbones, both compounds had two reduction processes, but the first reduction of **2DQTT-i** was irreversible (see Supporting Information). The LUMO energy levels are estimated to be −4.77 eV for **2DQTT-i**, −4.51 eV for **2DQTT-o**, and −4.75 eV for **QTT** by the empirical equation, LUMO = −(4.80 + E_{onset}) eV (E_{onset}: the onset of the reduction wave). Although both compounds are very stable in ambient solution and solid state, **2DQTT-o** should be more suitable to be applied as a stable n-type semiconductor because of its favorable LUMO energy level.[18]

Thin-Film Transistor Characterization of 2DQTTs and QTT. The potential of **2DQTT-i** and **2DQTT-o** for use in n-type OTFTs was investigated. Bottom-gate bottom-contact (BGBC) OTFT devices were fabricated on octadecyltrichlorosilane (OTS)-modified SiO_2 (300 nm)/Si substrates. Thin films (40−60 nm in thickness) were spin-coated as the organic semiconducting layer, and 30 nm gold served as the source−drain electrodes. The thin films were annealed at 80, 120, 160, 190, or 240 °C. Figure 4 shows the *I*−*V* characteristics of **2DQTT-i** and **2DQTT-o**. All the devices exhibit similar characteristics in air and under N_2 atmosphere, probably as a result of the deep LUMO energy level, with well-defined linear and saturation regimes. The device performances of **2DQTT-i** and **2DQTT-o** were collected and are summarized in Table 1. Devices based on **2DQTT-i** show a stepwise improvement of electron mobility with increasing annealing temperature ($\mu_{e(avg)}$ = 0.03 cm^2 V^{-1} s^{-1} at 80 °C; and $\mu_{e(avg)}$ = 0.14 cm^2 V^{-1} s^{-1} at 190 °C). A maximum mobility of 0.44 cm^2 V^{-1} s^{-1} was observed for an annealing temperature of 190 °C. **2DQTT-o**-based devices display a different trend compared with OTFTs based on **2DQTT-i**. No obvious increase in mobility was observed after annealing at a temperature lower than 120 °C. However, the mobility increased significantly from 0.05 cm^2 V^{-1} s^{-1} to a value well over 1.5 cm^2 V^{-1} s^{-1} after annealing at 160 °C. An exciting device performance with a maximum electron mobility of 3.0 cm^2 V^{-1} s^{-1} and I_{on}/I_{off} = 10^5 was achieved.[19] This performance makes **2DQTT-o** one of the best solution-processable air-stable n-channel semiconductors. By sharp contrast, **QTT** shows inferior electron mobilities, by as much as 4 orders of magnitude. Figure 5 shows the histograms of the electron mobility distribution for 24 OTFTs based on **2DQTT-i** and **2DQTT-o**, respectively. For **2DQTT-i**-based transistors most devices display moderate mobility higher than 0.1 cm^2 V^{-1} s^{-1}. As a comparison, all the OTFTs based **2DQTT-o** exhibit electron mobility higher than 0.8 cm^2 V^{-1} s^{-1},

dx.doi.org/10.1021/ja510003y | J. Am. Chem. Soc. 2014, 136, 16176−16184

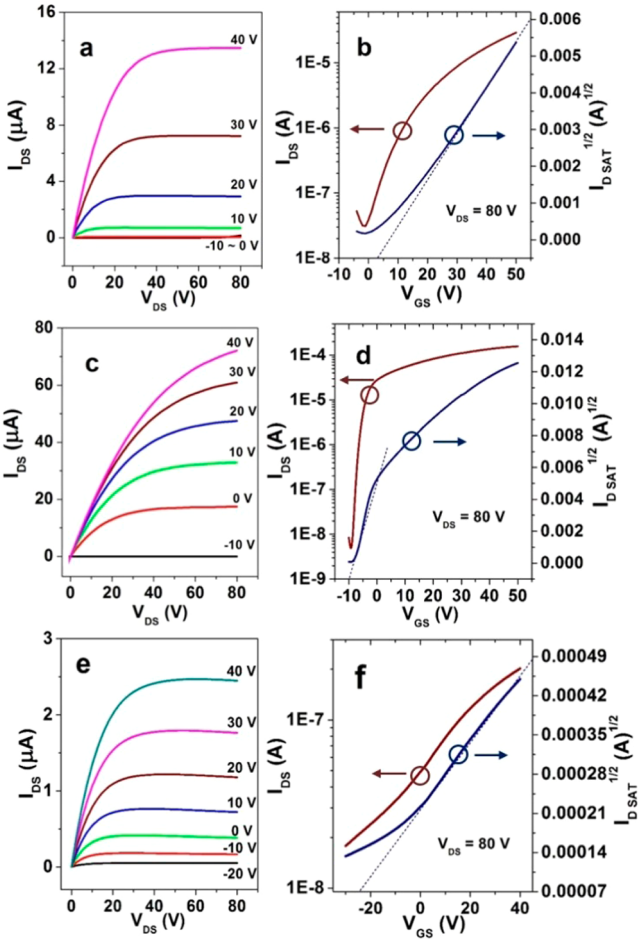

Figure 4. Output (a, c, e) and transfer (b, d, e) characteristics of BGBC OTFTs based on **2DQTT-i** (a, b), **2DQTT-o** (c, d), and **QTT** (e, f). Devices based on **2DQTT-i** and **2DQTT-o** were annealed at 190 and 160 °C, respectively.

while 25% devices show mobility higher than 2.0 $cm^2\ V^{-1}\ s^{-1}$. From these data we can meaningfully conclude that **2DQTT-o** possesses superior charge transport than that of **2DQTT-i**.[20] These results indicate that the orientation of the two fused TT subunits and balanced 2D structure have a significant influence on the carrier transport properties.

Thin-Film Morphology. To explore the annealing temperature-dependent performances of **2DQTT-i**- and **2DQTT-o**-based

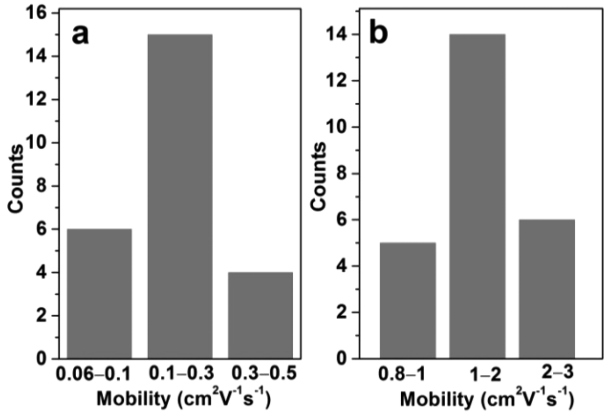

Figure 5. Histograms of device mobility for a set of OFETs based on **2DQTT-i** (a) and **2DQTT-o** (b), composed of 24 separate devices.

OTFTs, thin films of **2DQTT-i** and **2DQTT-o** were examined by atomic force microscopy (AFM) measurements. Figure 6 shows the AFM images of spin-coated films annealed at different temperatures (from 80 to 190 °C). No obvious change of film morphology of **2DQTT-i** was observed after annealing at a temperature lower than 160 °C, but enhanced lamellar ordering was observed after annealing at 190 °C. By comparison with the film morphology of the **2DQTT-i**, the **2DQTT-o**-based films appeared more crystalline with larger, more obvious domains that grow in size with increasing annealing temperature. An ordered film with large grain size (200−1000 nm) and terraced surface microstructure can be successfully obtained when annealed at 160 °C.

The two-dimensional grazing incidence wide-angle X-ray scattering (2D GIWAXS) images for **2DQTT-i** and **2DQTT-o** as a function of annealing temperature are shown in Figure 7. 2D GIWAXS investigations are consistent with our AFM studies. Out-of plane GIWAXS patterns of spin-coated thin films at room temeprature indicated strong first-order diffraction peaks with similar 2θ values of 4.93° (**2DQTT-o**) and 5.06° (**2DQTT-i**), which correspond to *d*-spacing of 17.9 and 17.5 Å, respectively. With increasing annealing temperature, the first-order diffraction peak became more intense with a higher-order diffraction peak observed at 9.8°, indicating increasing crystallinity of the thin films, contributing to the outstanding performances obtained under high annealing temperatures. Increasing annealing temperature results in a greater enhancement of lamellar peak intensity in films of **2DQTT-o** than that

Table 1. Maximum (Average) Electron Mobilities (μ_e)[a], Current On/Off Ratios (I_{on}/I_{off}), and Minimum (Average) Threshold Voltages (V_{Th}) for OTFT Devices Based on 2DQTT-i, 2DQTT-o, and QTT

semiconductor	annealing temperature (°C)	electron mobility (μ_e) ($cm^2\ V^{-1}\ s^{-1}$)	I_{on}/I_{off}	V_{Th} (V)
2DQTT-i	80	0.05 (0.03)	10^3 (10^3)	2.1 (6.4)
	120	0.05 (0.04)	10^3 (10^3)	0.8 (6.4)
	160	0.21 (0.1)	10^3 (10^3)	3.6 (9.3)
	190	0.44 (0.14)	10^3 (10^3)	2.6 (5.4)
	240	0.14 (0.1)	10^3 (10^3)	2.1 (8.7)
2DQTT-o	80	0.14 (0.05)	10^6 (10^5)	−15.2 (−19.8)
	120	0.12 (0.05)	10^4 (10^4)	−19.8 (−23)
	160	3.0 (1.51)	10^6 (10^5)	−1.4 (−11.1)
	190	0.74 (0.43)	10^6 (10^5)	−6.9 (−11)
QTT	80	0.0002 (0.0005)	10^2 (10^2)	−10.0 (−31.0)
	120	0.0003 (0.0005)	10 (10)	−26.3 (−52.1)

[a]Typical device characteristics obtained from 25 devices; all devices were measured under ambient conditions.

dx.doi.org/10.1021/ja510003y | J. Am. Chem. Soc. 2014, 136, 16176−16184

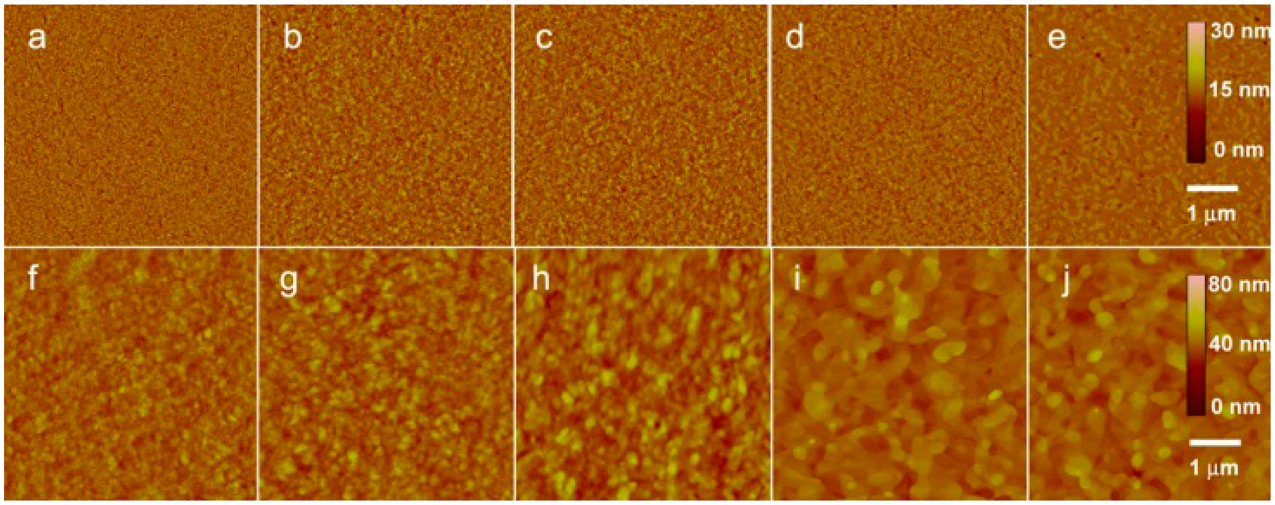

Figure 6. AFM images of thin films of **2DQTT-i** and **2DQTT-o** at room temperature (a, f) and after thermal annealing at temperatures of 80 °C (b, g), 120 °C (c, h), 160 °C (d, i), and 190 °C (e, j), respectively. (Upper panels: **2DQTT-i**, lower panels: **2DQTT-o**.)

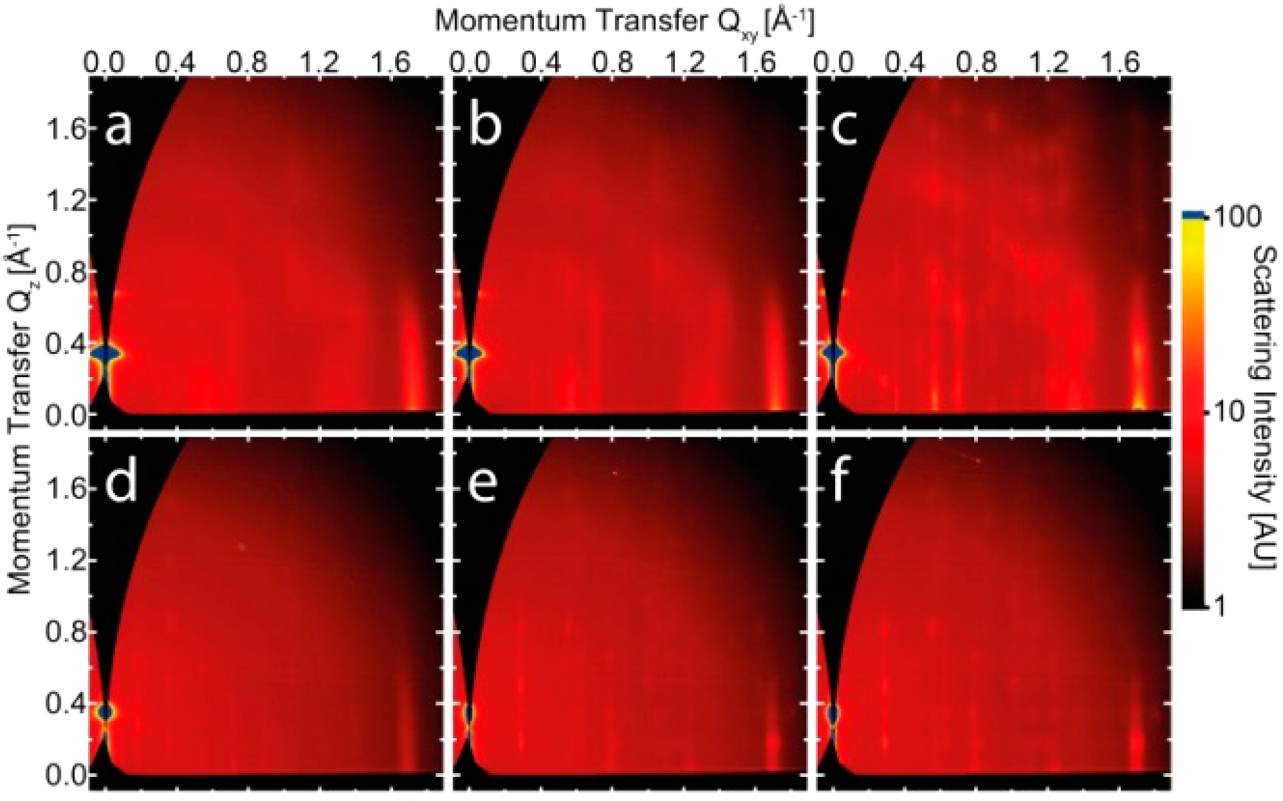

Figure 7. 2D GIWAXS patterns of **2DQTT-i** and **2DQTT-o** at different annealing temperatures of 120 °C (a, d), 160 °C (b, e), and 190 °C (c, f), respectively.

of **2DQTT-i**. By sharp contrast, X-ray diffraction (XRD) measurements of **QTT** (Figure S9) indicate amorphous aggregation of **QTT**, which may be responsible for the inferior OTFT performance. All of the results indicate varied crystalline properties of **QTT** derivatives induced by sulfur position in the molecules. 2D GIWAXS in addition collects the off-specular diffraction, importantly including the in-plane direction critical for charge transport in OTFTs, and the orientational width of each peak. Both **2DQTT-i** and **2DQTT-o** stack edge-on to the substrate with strongest reflections corresponding to alkyl stacking perpendicular to the substrate and a peak located in-plane at about 1.7 Å^{-1} which likely corresponds to $\pi-\pi$ stacking. With annealing, **2DQTT-i** largely maintains a single-crystal structure, the peaks of which become more intense, indicating an increase in overall crystallinity, and sharper, indicating an increased crystalline coherence length or larger crystals with annealing. The orientational full width at half-maximum (fwhm) of **2DQTT-i** steadily decreases from 6.4° at 120 °C to 4.3° and 190 °C. For **2DQTT-o** there exists a clear unit cell change with annealing from 120 to 160 °C (also observed in the corresponding AFM images) and increasing crystallinity with annealing to 190 °C. The orientational fwhm

dx.doi.org/10.1021/ja510003y | J. Am. Chem. Soc. 2014, 136, 16176−16184

decreases from 5.5° at 120 °C to 3.4° at both 160 and 190 °C. Compared with **2DQTT-i**, **2DQTT-o** shows much sharper peaks, indicative of larger crystalline coherence lengths and this higher degree of orientational order. Assuming the intense peak located in-plane at about 1.7 $Å^{-1}$ can be assigned to $\pi-\pi$ stacking, we evaluate a $\pi-\pi$ cofacial stacking distance of 3.4 Å for both compounds which is largely in agreement with the value from the single-crystal analysis of **2DQTT-o** discussed above. In summary, minor differences in the molecular structure of **2DQTT-i** and **2DQTT-o** significantly affect the molecular packing and thin-film morphology, which results in disparate OTFT performance.

Discussion. The construction of **2DQTT**s was successfully realized by the selective functionalization of unsymmetrical TT unit. The weak O−S and S−S intramolecular interactions resulted in **2DQTT-i** with exclusive *E*,*E*-configuration. Because of the absence of S−S interactions, a minor amount of the **2DQTT-o** isomer with *E*,*Z*-configuation can be visible in solution state in ^{1}H NMR spectrum. However, **2DQTT-o** showed exclusively the *E*,*E*-configuration in solid state as indicated by single-crystal X-ray analysis. Differing from the herringbone packing of linear **QOT**s, **2DQTT-o** showed favorable "brick-layer" arrangement[21] in bulk single-crystal state because of the expanded π-surface[12] and steric hindrance[22] of the branched 2-ethylhexyl groups attached on the central TPD unit. *J*-aggregation of **2DQTT-o** was clearly observed in the thin film revealing the slipped molecular arrangement. The LUMO energy level of **2DQTT-o** is proper (−4.51 eV) as a stable n-type semiconductor.

For typical organic semiconductor-based OTFTs, the carrier transport is mainly determined by the intermolecular charge transport inside the crystalline domains and the carrier trapping in the intergrain regions. As indicated by AFM images (Figure 6) and 2D GIWAXS (Figure 7), obvious differences in film morphology of **2DQTT-i** and **2DQTT-o** were observed. **2DQTT-o** film possesses larger domain size and crystalline coherence length when the annealing temperature reached 160 °C than that of **2DQTT-i** under same condition. In addition, the intermolecular stacking plays an important role in determining the device performances. With the aid of 2D GIWAXS measurements, we are able to gain further insight into the packing mode of **2DQTT**s in thin films. For many solution-processed organic semiconductors, different crystalline forms can exist, but single crystals of different phases are difficult to obtain.[23] In this case, although we obtained single crystals of **2DQTT-o**, we find the molecular packing extracted from the obtained single crystal does not match the intermolecular stacking seen in thin film by GIWAXS. The unit cells of **2DQTT-i** and **2DQTT-o** were calculated by fitting diffraction peaks and scattering backgrounds using a Levenberg−Marquardt nonlinear least-squares fitting method. **2DQTT-i** largely maintains the same crystal structure with annealing (with optimized unit cell parameters a = 19 Å, b = 17.5 Å, c = 11.25 Å, α = 90°, β = 80°, γ = 83°) with annealing leading to increasing crystalline coherence length (8.74 nm, 190 °C) and overall level of crystallinity. At 190 °C, however, a second minority crystal form with unidentified but much larger unit cell is also visible in the GIWAXS pattern from **2DQTT-i**, indicating a partial phase transition between 160 and 190 °C. (Figure S10). The optimized unit cell parameters of **2DQTT-o** (a = 11.3 Å, b = 37.5 Å, c = 21.54 Å, α = 90°, β = 90°, γ = 90°) are similar, although distinct from those found in bulk single-crystal measurements, with an approximate doubling of unit cell volume relative to the single-crystal measurements, indicating two molecules per unit cell in the thin film. In addition, **2DQTT-o** exhibits a phase change with annealing from a yet larger, but indistinct unit cell, to that given above when annealing from 120 to 160 °C, a transition also observed in the corresponding AFM images. **2DQTT-o** increases slightly in crystallinity with further annealing to 190 °C. However, thin films of **2DQTT-o** annealed at 160 °C give a better OTFT performance compared with annealing at 190 °C. One possibility for the decrease in performance, despite an apparent microstructural improvement, might be in-plane thermal expansion,[23b] which can produce microscopic defects when the **2DQTT-o** film was quenched from 190 °C to room temperature, but less when quenched from 160 °C. In any case, the morphology of the **2DQTT-o** thin film, with the lowest measured orientational disorder, and largest crystalline coherence length (9.89 nm) after annealing to 160 °C is most suitable for electron transfer. From OTFT characterization, **2DQTT-o** showed higher electron mobilities of up to 3.0 $cm^2\ V^{-1}\ s^{-1}$ than that of **2DQTT-i** by one order of magnitude. By contrast, the reference **QTT** with unbalanced 2D structure showed much inferior electron mobilities of low to $10^{-4}\ cm^2\ V^{-1}\ s^{-1}$. Thus, for organic semiconductors with asymmetric monomer units, TT in our case, the molecular regiochemistry may significantly affect the device performance and should be paid extra attention in molecular design toward organic semiconductors with prominent charge transport properties.[24]

■ CONCLUSION

In conclusion, we have developed new 2D π-expanded quinoidal terthiophenes, **2DQTT-i** and **2DQTT-o**, based on highly selective synthetic strategy. Both compounds showed distinctive 2D molecular structures with enhanced configuration stability because of the weak S−O and/or S−S intramolecular muli-interactions. Because of the A−D−A−D−A electronic structure, the LUMO energy levels of 2DQTTs are adequately low for applications in ambient-stable n-OTFTs and gave electron mobilities at the $10^{-1}\ cm^2\ V^{-1}\ s^{-1}$ level. The minor change of thiophene orientation in **2DQTT-i** and **2DQTT-o** significantly affected film morphology that resulted in different OTFT performances: 0.44 $cm^2\ V^{-1}\ s^{-1}$ (**2DQTT-i**) compared with 3.0 $cm^2\ V^{-1}\ s^{-1}$ (**2DQTT-o**). Higher crystallinity, longer crystalline coherence lengths, and the lowest orientational disorder of the crystalline structure of **2DQTT-o** compared to **2DQTT-i** accounts for its superior semiconductivity. As the reference, **QTT** with umbalanced 2D structure showed much inferior electron mobilities of low to $10^{-4}\ cm^2\ V^{-1}\ s^{-1}$. To the best of our knowledge, **2DQTT-o** is the first example among **QOT**s that exhibits an electron mobility surpassing 1.0 $cm^2\ V^{-1}\ s^{-1}$, revealing the potential of **2DQOT**-framework for constructing n-type organic semiconductors that can rival or even surpass state-of-the-art rylene diimides via proper molecular design.[25]

■ EXPERIMENTAL SECTION

Materials and General Methods. All the reactions dealing with air- or moisture-sensitive compounds were carried out in a dry reaction vessel under a positive pressure of nitrogen. Unless stated otherwise, starting materials were obtained from Adamas, Aldrich, and J&K and were used without any further purification. Anhydrous THF, toluene, and 1,4-dioxane were distilled over Na/benzophenone prior to use. Anhydrous DMF was distilled over CaH_2 prior to use. 2-Hexylthieno[3,4-*b*]thiophene (**1**),[15] 1,3-dibromo-5-(2-ethylhexyl)-4*H*-thieno[3,4-*c*]-pyrrole-4,6(5*H*)-dione (**3**), and 1,3-bis(5-bromothiophen-2-yl)-5-(2-ethylhexyl)-4*H*-thieno[3,4-*c*]pyrrole-4,6(5*H*)-dione (**9**)[26] were prepared according to the published procedures. Hydrogen nuclear magnetic

dx.doi.org/10.1021/ja510003y | J. Am. Chem. Soc. 2014, 136, 16176−16184

resonance (^{1}H NMR) and carbon nuclear magnetic resonance (^{13}C NMR) spectra were measured on BRUKER AVANCE 300 and BRUKER DMX 400 spectrometers. Chemical shifts for hydrogens are reported in parts per million (ppm, δ scale) downfield from tetramethylsilane and are referenced to the residual protons in the NMR solvent ($CDCl_3$: δ 7.26). ^{13}C NMR spectra were recorded at 100 MHz. Chemical shifts for carbons are reported in parts per million (ppm, δ scale) downfield from tetramethylsilane and are referenced to the carbon resonance of the solvent ($CDCl_3$: δ 77.0). The data are presented as follows: chemical shift, multiplicity (s = singlet, d = doublet, t = triplet, m = multiplet and/or multiple resonances, br = broad), coupling constant in Hertz (Hz), and integration. EI-MS measurements were performed on UK GCT-Micromass or SHIMADZU G-MS-QP2010 spectrometers. MALDI-TOF measurements were performed on an Applied Biosystems 4700 Proteomics Analyzer. Elemental analyses were measured on a Carlo Erba 1106 elemental analyzer. UV−vis spectra were recorded on a JASCO V-570 spectrometer. Cyclic voltammetry (CV) was performed on a CHI620D potentiostat. All measurements were carried out in a one-compartment cell under N_2 atmosphere, equipped with a glassy-carbon electrode, a platinum counter electrode, and a Ag/Ag^+ reference electrode. The supporting electrolyte was a 0.1 mol/L dichloromethane solution of tetrabutylammonium perchlorate (TBAP). All potentials were corrected against Fc/Fc^+. CV was measured with a scan rate of 100 mV/s. Thermogravimetric analysis (TGA) was performed on a Shimadzu DTG 60 instrument at a heating rate of 10 °C min^{-1} under a N_2 atmosphere with runs recorded from room temperature to 550 °C. X-ray crystallographic data were collected with a Bruker Smart CCD diffractometer through using graphite-monochromated Mo Kα radiation (λ = 0.71073 M).

*Tributyl(2-hexylthieno[3,4-b]thiophen-6-yl)stannane (**2**).* Compound **1** (0.49 g, 2.18 mmol) was dissolved in anhydrous THF (8 mL) under nitrogen atmosphere and cooled to −78 °C, and then *n*-butyllithium (1.50 mL, 2.40 mmol, 1.60 M in hexane) was added via syringe under stirring. After stirring at −78 °C for 0.5 h, tributyltin chloride (0.65 mL, 2.50 mmol) was added in one portion and stirred at −78 °C for another 0.5 h. The clear reaction solution was warmed to room temperature for 0.5 h. A few drops of saturated NH_4Cl solution was added to the reaction mixture and extracted three times with CH_2Cl_2. The organic layer was separated, dried over $MgSO_4$, and concentrated under reduced pressure. 1.18 g of compound **2** was obtained as light yellow oil in 99% yield and was directly used for the next step without further purification. ^{1}H NMR (400 MHz, $CDCl_3$): δ 0.86−0.92 (m, 12H), 1.11−1.71 (m, 26H), 2.76 (t, ^3J = 7.2 Hz, 2H), 6.65 (s, 1H), 7.40 (s, 1H); EI-MS: 514 $[M]^+$.

*5-(2-Ethylhexyl)-1,3-bis(2-hexylthieno[3,4-b]thiophen-6-yl)-4H-thieno[3,4-c]pyrrole-4,6(5H)-dione (**3**).* To an oven-dried round-bottomed flask loaded with compound **2** (1.10 g, 2.14 mmol) in anhydrous DMF (6 mL) and toluene (6 mL) under nitrogen atmosphere was added TPD-2Br (0.412 mg, 0.97 mmol) and $Pd(PPh_3)_4$ (45 mg, 0.039 mmol). The reaction was stirred and refluxed for 2 days under dark. The reaction mixture was then cooled to room temperature, and the product was precipitated. Pure **3** was collected by filtration and washed with MeOH (20 mL) as a brown solid (0.65 g, 94%). ^{1}H NMR (400 MHz, $CDCl_3$): δ 0.83−0.93 (m, 12H), 1.26−1.44 (m, 20H), 1.73−1.81 (m, 4H), 1.94 (br, 1H), 2.83−2.91 (m, 4H), 3.58 (d, ^3J = 7.2 Hz, 2H), 6.70 (s, 2H), 7.41 (s, 2H); ^{13}C NMR (100 MHz, $CDCl_3$): δ 10.5, 14.1, 22.6, 23.1, 23.9, 28.6, 28.8, 30.3, 30.6, 31.6, 31.8, 38.2, 42.5, 113.8, 115.6, 118.8, 126.9, 135.3, 139.8, 147.5, 153.6, 163.0; MS (MALDI-TOF): 709.3 $[M]^+$; Anal. calcd for $C_{38}H_{47}NO_2S_5$ (%): C, 64.27; H, 6.67; N, 1.97; Found (%): C, 64.36; H, 6.70; N, 2.03.

*1,3-Bis(4-bromo-2-hexylthieno[3,4-b]thiophen-6-yl)-5-(2-ethylhexyl)-4H-thieno[3,4-c]pyrrole-4,6(5H)-dione (**4**).* To a solution of compound **3** (0.40 g, 0.56 mmol) in $CHCl_3$/DMF (3:1, 16 mL) was added NBS (0.22 g, 1.24 mmol) in one portion. The reaction mixture was stirred at room temperature in dark for 2 h. The reaction mixture was washed with saturated NaCl solution (20 mL), saturated $NaHSO_3$ solution (20 mL), and saturated $NaCO_3$ solution (20 mL) successively, and the organic layer was dried over $MgSO_4$. After filtration, the solvent was removed under reduced pressure to afford crude product, which was further purified on a silica-gel column chromatography with CH_2Cl_2/petroleum ether (1:2) as the eluent. Compound **4** was obtained as a dark brown solid (0.43 g, 88%). ^{1}H NMR (400 MHz, $CDCl_3$): δ 0.83−0.94 (m, 12H), 1.25−1.45 (m, 20H), 1.74−1.81 (m, 4H), 1.91 (br, ^{1}H), 2.81−2.85 (m, 4H), 3.54 (d, ^3J = 7.6 Hz, 2H), 6.60 (s, 2H); ^{13}C NMR (100 MHz, $CDCl_3$): δ 10.6, 14.1, 22.6, 23.1, 24.0, 28.7, 28.89, 28.93, 29.9, 30.7, 31.6, 31.8, 38.3, 42.6, 103.6, 112.8, 120.0, 126.5, 134.0, 138.0, 147.2, 154.7, 162.7; MS (MALDI-TOF): 867.2 $[M]^+$; Anal. calcd for $C_{38}H_{45}Br_2NO_2S_5$ (%): C, 52.59; H, 5.23; N, 1.61; Found (%): C, 52.35; H, 5.30; N, 1.50.

*2,2′-((6E,6′E)-6,6′-(5-(2-ethylhexyl)-4,6-dioxo-5,6-dihydro-1H-thieno[3,4-c]pyrrole-1,3(4H)-diylidene)bis(2-hexylthieno[3,4-b]-thiophene-6,4(6H)-diylidene))dimalononitrile (**2DQTT-i**).* Sodium hydride (66 mg, 2.77 mmol) was added to a suspension of malononitrile (55 mg, 0.83 mmol) in anhydrous dioxane (10 mL) under nitrogen atmosphere and stirred for 10 min at room temperature. To this mixture was added compound **4** (0.30 g, 0.35 mmol) and $Pd(PPh_3)_4$ (40 mg, 0.035 mmol), which was then heated to reflux. After 4 h, the reaction was cooled to room temperature, and diluted hydrochloric acid (1M, 10 mL) and DDQ (118 mg, 0.52 mmol) were added and stirred at room temperature for 30 min. The resulting mixture was extracted with CH_2Cl_2 (3 × 50 mL), washed with brine, and dried over $MgSO_4$. After evaporation of the solvent, the residue was purified on a silica-gel column chromatography with CH_2Cl_2 followed by recrystallization twice in $CHCl_3/CH_3OH$ to give 0.205 g of **2DQTT-i** as a dark red solid in 71% yield. ^{1}H NMR (300 MHz, $CDCl_3$): δ 0.93−0.95 (m, 12H), 1.36−1.48 (m, 20H), 1.80−1.88 (m, 5H), 3.01−3.06 (m, 4H), 3.52 (d, ^3J = 7.2 Hz, 2H), 7.66 (s, 2H); ^{13}C NMR (75 MHz, $CDCl_3$): δ 10.5, 14.1, 22.6, 23.1, 24.0, 28.6, 28.9, 30.6, 31.1, 31.5, 32.0, 38.3, 43.3, 68.4, 113.2, 113.6, 119.3, 127.8, 141.4, 144.3, 146.2, 161.8, 162.3, 162.4; MS (MALDI-TOF): 835.2 $[M]^+$; Anal. calcd for $C_{44}H_{45}N_5O_2S_5$ (%): C, 63.20; H, 5.42; N, 8.38; Found (%): C, 62.93; H, 5.40; N, 8.45.

*2-Hexyl-4,6-diiodothieno[3,4-b]thiophene (**5**).* To a solution of compound **1** (2.02 g, 9.0 mmol) in $CHCl_3$ (100 mL) was added NIS (4.45 g, 19.8 mmol) in one portion with a few drops of CF_3COOH and was stirred at room temperature in dark for 2 h. The reaction mixture was washed with saturated NaCl solution (100 mL), saturated $NaHSO_3$ solution (100 mL), and saturated $NaCO_3$ solution (100 mL) successively and was then dried over $MgSO_4$. After evaporation of the solvent, the crude product was purified on a silica-gel column chromatography with petroleum ether as the eluent. Compound **5** was obtained as a light yellow solid (2.06 g, 48%). ^{1}H NMR (400 MHz, $CDCl_3$): δ 0.88−0.92 (m, 3H), 1.29−1.40 (m, 6H), 1.54−1.72 (m, 2H), 2.72−2.76 (m, 2H), 6.53 (s, 1H); ^{13}C NMR (100 MHz, $CDCl_3$): δ 14.2, 22.6, 28.8, 30.2, 31.6, 32.2, 60.3, 60.4, 115.5, 137.5, 145.8, 155.2; EI−MS: 476 $[M]^+$; Anal. calcd for $C_{12}H_{14}I_2S_2$ (%): C, 30.27; H, 2.96; Found (%): C, 30.42; H, 3.10.

*Tributyl(2-hexylthieno[3,4-b]thiophen-4-yl)stannane (**6**).* Compound **5** (1.62 g, 3.39 mmol) was dissolved in anhydrous THF (15 mL) under nitrogen atmosphere, and *n*-butyllithium (2.33 mL, 3.73 mmol, 1.6 M in hexane) was added dropwise via syringe under stirring at −78 °C. After stirring for 0.5 h, H_2O (2 mL) was added, and the reaction was warmed to room temperature. The reaction mixture was extracted three times with CH_2Cl_2. The organic layer was separated, dried over $MgSO_4$, and concentrated under reduced pressure. The resulting 2-hexyl-4-iodothieno[3,4-*b*]thiophene (1.10 g, 3.13 mmol) was dissolved in anhydrous THF (15 mL) under nitrogen atmosphere and cooled to −78 °C again. *n*-Butyllithium (2.25 mL, 3.60 mmol, 1.6 M in hexane) was added dropwise via syringe under stirring. After stirring at −78 °C for 0.5 h, tributyltin chloride (0.98 mL, 3.44 mmol) was added in one portion. After stirring at −78 °C for another 0.5 h, the cooling bath was removed, and the clear reaction solution was warmed to room temperature for another 0.5 h. A few drops of saturated NH_4Cl solution were added, and the mixture was extracted three times with CH_2Cl_2. The organic layer was separated, dried over $MgSO_4$, and concentrated under reduced pressure. Compound **6** was obtained as light yellow oil, which was used for the next step without further purification (1.81 g, 99%). ^{1}H NMR (400 MHz, $CDCl_3$): δ

dx.doi.org/10.1021/ja510003y | J. Am. Chem. Soc. 2014, 136, 16176−16184

0.88−0.94 (m, 12H), 1.11−1.71 (m, 26H), 2.76 (t, ^3J = 7.2 Hz, 2H), 6.53 (s, 1H), 7.42 (s, 1H); EI-MS: 514 $[M]^+$.

*5-(2-Ethylhexyl)-1,3-bis(2-hexylthieno[3,4-b]thiophen-4-yl)-4H-thieno[3,4-c]pyrrole-4,6(5H)-dione (**7**).* Compound **7** was synthesized following the same procedure as compound **3** starting from **6** (1.61 g, 3.13 mmol), TPD-2Br (0.61 g, 1.44 mmol), and $Pd(PPh_3)_4$ (67 mg, 0.058 mmol). Compound **7** was obtained as brown solid (0.723 g, 71%). ^{1}H NMR (300 MHz, $CDCl_3$): δ 0.89−0.94 (m, 12H), 1.32−1.43 (m, 20H), 1.73−1.83 (m, 4H),1.87 (br, 1H), 2.84−2.92 (m, 4H), 3.57 (d, ^3J = 7.2 Hz, 2H), 7.03 (s, 2H), 7.38 (s, 2H); ^{13}C NMR (100 MHz, $CDCl_3$): δ 10.5, 14.1, 22.6, 23.1, 23.9, 28.6, 28.8, 30.4, 30.6, 31.6, 32.3, 38.2, 42.4, 114.6, 115.1, 117.5, 127.3, 135.6, 139.5, 146.6, 157.0, 162.9; MS (MALDI-TOF): 709.2 $[M]^+$; Anal. calcd for $C_{38}H_{47}NO_2S_5$ (%): C, 64.27; H, 6.67; N, 1.97; Found (%): C, 64.40; H, 6.63; N, 2.00.

*1,3-Bis(4-bromo-2-hexylthieno[3,4-b]thiophen-4-yl)-5-(2-ethylhexyl)-4H-thieno[3,4-c]pyrrole-4,6(5H)-dione (**8**).* Compound **8** was synthesized following the same procedure as compound **4** starting from **7** (0.40 g, 0.56 mmol) and NBS (0.22 g, 1.24 mmol). Compound **8** was obtained as a dark brown solid (0.41 g, 84%). ^{1}H NMR (400 MHz, $CDCl_3$): δ 0.89−0.94 (m, 12H), 1.30−1.43 (m, 20H), 1.69−1.84 (m, 4H), 1.86 (br, 1H), 2.85−2.88 (m, 4H), 3.56 (d, ^3J = 7.2 Hz, 2H), 7.01 (s, 2H); ^{13}C NMR (100 MHz, $CDCl_3$): δ 10.5, 14.1, 22.6, 23.1, 23.9, 28.6, 28.8, 30.3, 30.6, 31.6, 32.4, 38.2, 42.5, 103.4, 115.4, 119.0, 127.1, 134.3, 141.2, 145.5, 157.8, 162.7; MS (MALDI-TOF): 867.0 $[M]^+$; Anal. calcd for $C_{38}H_{45}Br_2NO_2S_5$ (%): C, 52.59; H, 5.23; N, 1.61; Found (%): C, 52.72; H, 5.35; N, 1.58.

*2,2′-((4E,4′E)-4,4′-(5-(2-ethylhexyl)-4,6-dioxo-5,6-dihydro-1H-thieno[3,4-c]pyrrole-1,3(4H)-diylidene)bis(2-hexylthieno[3,4-b]-thiophene-6,4(4H)-diylidene))dimalononitrile (**2DQTT-o**).* Compound **2DQTT-o** was synthesized following the same procedure as for **2DQTT-i** starting from compound **8** (0.30 g, 0.35 mmol), malononitrile (55 mg, 0.83 mmol), sodium hydride (66 mg, 2.77 mmol), and $Pd(PPh_3)_4$ (40 mg, 0.035 mmol). **2DQTT-o** was obtained as a dark red solid (0.18 g, 63%). ^{1}H NMR (400 MHz, $CDCl_3$): δ 0.90−0.96 (m, 12H), 1.32−1.48 (m, 20H), 1.82−1.89 (m, 5H), 3.03−3.07 (m, 4H), 3.55 (d, ^3J = 7.2 Hz, 2H), 7.26 (s, 2H, 86% for isomer I), 7.31 (s, 1H, 14% for isomer II), 7.66 (s, 1H, 14% for isomer II); ^{13}C NMR (125 MHz, $CDCl_3$): δ 10.4, 14.0, 22.5, 23.0, 23.9, 28.5, 28.8, 30.9, 31.5, 32.1, 38.2, 43.3, 65.8, 113.3, 113.9, 119.2, 127.5, 128.9, 139.6, 142.7, 150.9, 161.8, 161.9, 163.8; MS (MALDI-TOF): 835.3 $[M]^+$; Anal. calcd for $C_{44}H_{45}N_5O_2S_5$ (%): C, 63.20; H, 5.42; N, 8.38; Found (%): C, 63.10; H, 5.18; N, 8.49.

*2,2′-((5E,5′E)-5,5′-(5-(2-ethylhexyl)-4,6-dioxo-5,6-dihydro-1H-thieno[3,4-c]pyrrole-1,3(4H)-diylidene)bis(thiophene-5,2(5H)-diylidene))dimalononitrile (**QTT**).* **QTT** was synthesized following the same procedure as for **2DQTT-i** starting from **9** (0.20 g, 0.35 mmol), malononitrile (55 mg, 0.83 mmol), sodium hydride (66 mg, 2.77 mmol), and $Pd(PPh_3)_4$ (40 mg, 0.035 mmol). **QTT** was obtained as a dark blue solid (97 mg, 51%). ^{1}H NMR (400 MHz, $CDCl_3$): δ 0.69−0.95 (m, 6H), 1.34−1.37 (m, H), 1.78 (br, 1H), 3.58 (d, ^3J = 6.8 Hz, 2H), 7.47 (br, 2H), 8.84 (s, 2H); MS (MALDI-TOF): 555.1 $[M]^+$; Anal. calcd for $C_{28}H_{21}N_5O_2S_3$ (%): C, 60.52; H, 3.81; N, 12.60; Found (%): C, 60.46; H, 3.83; N, 12.51.

Device Fabrication and Measurements of OTFTs. A heavily doped Si wafer with a 300 nm SiO_2 served as the gate electrode and dielectric layer, respectively. Thirty nm Au electrodes were deposited and patterned by a typical lift-off technique with channel length ranging from 5−50 μm and channel width of 1.4 mm. The OTS modification was carried out in a vacuum oven at a temperature of 120 °C for 3 h. The treated substrates were rinsed successively with hexane, ethanol, and chloroform, respectively. The organic active layer was deposited on the OTS-treated substrates by a spin-coating process of their chloroform solutions, which followed by the annealing treatments at varied temperatures.

Thin-Film Characterization. X-Ray diffraction (XRD) measurements of thin films were performed in reflection mode at 40 kV and 200 mA with Cu Kα radiation using a 2 kW Rigaku X-ray diffractometer. AFM images of the thin films were obtained on a NanoscopeIIIa AFM (Digital Instruments) operating in tapping mode. GIWAXS measurements were performed at the SAXS/WAXS beamline of the Australian Synchrotron.[27] 9 keV Photons were used with 2D scattering patterns recorded by a Pilatus 1 M detector. The sample-to-detector distance was calibrated using a silver behenate standard. Scattering patterns were recorded as a function of X-ray angle of incidence, with the angle of incidence varying from 0.05° below the critical angle of the organic film to 0.2° above the critical angle. The images reported were at the critical angle as identified by the angle with the highest scattering intensity. Data acquisition times of 3 s were used, with three 1 s exposures taken with offset detector positions to cover gaps in the Pilatus detector. XRD data are expressed as a function of the scattering vector, **q**, that has a magnitude of $(4\pi/\lambda)\sin(\theta)$, where θ is half the scattering angle and λ is the wavelength of the incident radiation.

■ ASSOCIATED CONTENT

Supporting Information

Physical properties, single-crystal analysis, detailed 2D GIWAX patterns, and NMR spectra of **2DQTT-i**, **2DQTT-o**, and **QTT**, cif file of **2DQTT-o**. This material is available free of charge via the Internet at http://pubs.acs.org.

■ AUTHOR INFORMATION

Corresponding Authors

xzzhu@iccas.ac.cn

dicha@iccas.ac.cn

Notes

The authors declare no competing financial interest.

■ ACKNOWLEDGMENTS

We thank the National Basic Research Program of China (973 Program) (No. 2014CB643502) for financial support, the Strategic Priority Research Program of the Chinese Academy of Sciences (XDB12010200), and National Natural Science Foundation of China (91333113). C.R.M. acknowledges support from the Australian Research Council (FT100100275, DP130102616) and thanks Dr. Nigel Kirby of the Australian Synchrotron for technical support.

■ REFERENCES

(1) (a) Zhao, Y.; Guo, Y.; Liu, Y. *Adv. Mater.* **2013**, *25*, 5372. (b) Anthony, J. E.; Facchetti, A.; Heeney, M.; Marder, S. R.; Zhan, X. *Adv. Mater.* **2010**, *22*, 3876. (c) Wang, C.; Dong, H.; Hu, W.; Liu, Y.; Zhu, D. *Chem. Rev.* **2011**, *112*, 2208. (d) Usta, H.; Facchetti, A.; Marks, T. J. *Acc. Chem. Soc.* **2011**, *44*, 501. (e) Mei, J.; Diao, Y.; Appleton, A. L.; Fang, L.; Bao, Z. *J. Am. Chem. Soc.* **2013**, *135*, 6724. (f) Usta, H.; Facchetti, A.; Marks, T. *Acc. Chem. Res.* **2011**, *44*, 501.

(2) (a) Guillaud, G.; Alsadoun, M.; Maitrot, M.; Simon, J.; Bouvet, M. *Chem. Phys. Lett.* **1990**, *167*, 503. (b) Mallik, A. B.; Locklin, J.; Mannsfeld, S. C. B.; Reese, C.; Roberts, M. E.; Senatore, M. L.; Zi, H.; Bao, Z. In *Organic Field-Effect Transistors*; Bao, Z., Locklin, J. J., Eds.; CRC Press: Boca Raton, FL, 2007; p 159−228.

(3) (a) Rappenfus, T. M.; Chesterfield, R. J.; Frisbie, C. D.; Mann, K. R.; Casado, J.; Raff, J. D.; Miller, L. L. *J. Am. Chem. Soc.* **2002**, *124*, 4184. (b) Casado, J.; Ortiz, R. P.; Navarrete, J. T. L. *Chem. Soc. Rev.* **2012**, *41*, 5672.

(4) (a) Handa, S.; Miyazaki, E.; Takimiya, K.; Kunugi, Y. *J. Am. Chem. Soc.* **2007**, *129*, 11684. (b) Suzuki, Y.; Miyazaki, E.; Takimiya, K. *J. Am. Chem. Soc.* **2010**, *132*, 10453. (c) Ribierre, J. C.; Fujihara, T.; Watanabe, S.; Matsumoto, M.; Muto, T.; Nakao, A.; Aoyama, T. *Adv. Mater.* **2010**, *22*, 1722. (d) Wu, Q.; Ren, S.; Wang, M.; Qiao, X.; Li, H.; Gao, X.; Yang, X.; Zhu, D. *Adv. Funct. Mater.* **2013**, *23*, 2277. (e) Qiao, Y.; Guo, Y.; Yu, C.; Zhang, F.; Xu, W.; Liu, Y.; Zhu, D. *J. Am. Chem. Soc.* **2012**, *134*, 4084.

(5) Wu, Q.; Li, R.; Hong, W.; Li, H.; Gao, X.; Zhu, D. *Chem. Mater.* **2011**, *23*, 3138.

(6) (a) Handa, S.; Miyazaki, E.; Takimiya, K. *Chem. Commun.* **2009**, 3919. (b) Pappenfus, T. M.; Hermanson, B. J.; Helland, T. J.; Lee, G. G. W.; Drew, S. M.; Mann, K. R.; McGee, K. A.; Rasmussen, S. C. *Org. Lett.* **2008**, *10*, 1553.
(7) (a) Gao, X.; Di, C.-a.; Hu, Y.; Yang, X.; Fan, H.; Zhang, F.; Liu, Y.; Li, H.; Zhu, D. *J. Am. Chem. Soc.* **2010**, *132*, 3697. (b) Zhan, X.; Facchetti, A.; Barlow, S.; Marks, T. J.; Ratner, M. A.; Wasielewski, M. R.; Marder, S. R. *Adv. Mater.* **2011**, *23*, 268. (c) Liu, Z.; Zhang, G.; Cai, Z.; Chen, X.; Luo, H.; Li, Y.; Wang, J.; Zhang, D. *Adv. Mater.* **2014**, *26*, 6965.
(8) (a) Huang, C.; Barlow, S.; Marder, S. R. *J. Org. Chem.* **2011**, *76*, 2386. (b) Schmidt, R.; Oh, J. H.; Sun, Y.-S.; Deppisch, M.; Krause, A.-M.; Radacki, K.; Braunschweig, H.; Könemann, M.; Erk, P.; Bao, Z.; Würthner, F. *J. Am. Chem. Soc.* **2009**, *131*, 6215. (c) Lv, A.; Puniredd, S. R.; Zhang, J.; Li, Z.; Zhu, H.; Jiang, W.; Dong, H.; He, Y.; Jiang, L.; Li, Y.; Pisula, W.; Meng, Q.; Hu, W.; Wang, Z. *Adv. Mater.* **2012**, *24*, 2626.
(9) Coropceanu, V.; Cornil, J.; da Silva Filho, D. A.; Olivier, Y.; Silbey, R.; Brédas. *Chem. Rev.* **2007**, *107*, 926.
(10) Liang, Y.; Yu, L. *Acc. Chem. Res.* **2010**, *43*, 1227.
(11) (a) Pron, A.; Berrouard, P.; Leclerc, M. *Macromol. Chem. Phys.* **2013**, *214*, 7. (b) Zou, Y.; Najari, A.; Berrouard, P.; Beaupré, S.; Badrou, R. A.; Tao, Y.; Leclerc, M. *J. Am. Chem. Soc.* **2010**, *132*, 5330. (c) Piliego, C.; Holcombe, T. W.; Douglas, J. D.; Woo, C. H.; Beaujuge, P. M.; Fréchet, J. M. J. *J. Am. Chem. Soc.* **2010**, *132*, 7595.
(12) (a) Debije, M. G.; Piris, J.; de Haas, M. P.; Warman, J. M.; Tomovic, Z.; Simpson, C. D.; Watson, M. D.; Müllen, K. *J. Am. Chem. Soc.* **2004**, *126*, 4641. (b) Feng, X.; Marcon, V.; Pisula, W.; Hansen, M. R.; Kirkpatrick, J.; Grozema, F.; Andrienko, D.; Kremer, K.; Müllen, K. *Nat. Mater.* **2009**, *8*, 421.
(13) (a) Jackson, N. E.; Savoie, B. M.; Kohlstedt, K. L.; de la Cruz, M. O.; Schatz, G. C.; Chen, L. X.; Ratner, M. A. *J. Am. Chem. Soc.* **2013**, *135*, 10475. (b) Pomerantz, M. *Tetrahedron Lett.* **2003**, *44*, 1563. (c) Turbiez, M.; Frère, P.; Allain, M.; Videlot, C.; Ackermann, J.; Roncali, J. *Chem.—Eur. J.* **2005**, *11*, 3742. (d) Guo, X.; Kim, F. S.; Jenekhe, S. A.; Watson, M. D. *J. Am. Chem. Soc.* **2009**, *131*, 7206. (e) Berrouard, P.; Grenier, F.; Pouliot, J.-R.; Gagnon, E.; Tessier, C.; Leclerc, M. *Org. Lett.* **2011**, *13*, 38. (f) Guo, X.; Ortiz, R. P.; Zheng, Y.; Kim, M.-G.; Zhang, S.; Hu, Y.; Lu, G.; Facchetti, A.; Marks, T. J. *J. Am. Chem. Soc.* **2011**, *133*, 13685. (g) Huang, H.; Chen, Z.; Ortiz, R. P.; Newman, C.; Usta, H.; Lou, S.; Youn, J.; Noh, Y.-Y.; Baeg, K.-J.; Chen, L. X.; Facchetti, A.; Marks, T. *J. Am. Chem. Soc.* **2012**, *134*, 10966. (h) Guo, X.; Zhou, N.; Lou, S. J.; Hennek, J. W.; Ortiz, R. P.; Butler, M. R.; Boudreault, P.-L. T.; Strzalka, J.; Morin, P.-O.; Leclerc, M.; Navarrete, J. T. L.; Ratner, M. A.; Chen, L. X.; Chang, R. P. H.; Facchetti, A.; Marks, T. J. *J. Am. Chem. Soc.* **2012**, *134*, 18427. (i) Guo, X.; Quinn, J.; Chen, Z.; Usta, H.; Zheng, Y.; Xia, Y.; Hennek, J. W.; Ortiz, R. P.; Marks, T. J.; Facchetti, A. *J. Am. Chem. Soc.* **2013**, *135*, 1986.
(14) (a) Zhang, F.; Hu, Y.; Schuettfort, T.; Di, C.-a.; Gao, X.; McNeill, C. R.; Thomsen, L.; Mannsfeld, S. C. B.; Yuan, W.; Sirringhaus, H.; Zhu, D. *J. Am. Chem. Soc.* **2013**, *135*, 2338. (b) Pei, T.; Wang, J.-Y.; Pei, J. *Chem. Mater.* **2014**, *26*, 594. (c) Mei, J.; Bao, Z. *Chem. Mater.* **2014**, *26*, 604.
(15) Patra, A.; Wijsboom, Y. H.; Leitus, G.; Bendikov, M. *Chem. Mater.* **2011**, *23*, 896.
(16) Higuchi, H.; Nakayama, T.; Koyama, H.; Ojima, J.; Wada, T.; Sasabe, H. *Bull. Chem. Soc. Jpn.* **1995**, *68*, 2363.
(17) (a) Würthner, F.; Kaiser, T. E.; Saha-Möller, C. R. *Angew. Chem., Int. Ed.* **2011**, *50*, 3376. (b) Gsänger, M.; Kirchner, E.; Stolte, M.; Burschka, C.; Stepanenko, V.; Pflaum, J.; Würthner, F. *J. Am. Chem. Soc.* **2014**, *136*, 2351.
(18) (a) Usta, H.; Risko, C.; Wang, Z.; Huang, H.; Deliomeroglu, M. K.; Zhukhovitskiy, A.; Facchetti, A.; Marks, T. J. *J. Am. Chem. Soc.* **2009**, *131*, 5586. (b) Ye, Q.; Chang, J.; Huang, K.-W.; Shi, X.; Wu, J.; Chi, C. *Org. Lett.* **2013**, *15*, 1194.
(19) As the factors influencing threshold voltages are quite varied, we preliminarily attribute the different threshold voltages to the different packing patterns of **2DQTT-i** and **2DQTT-o**; see: Veres, J.; Ogier, S.; Lloyd, G.; de Leeuw, D. *Chem. Mater.* **2004**, *16*, 4543.
(20) Luber, E. J.; Buriak, J. M. *ACS Nano* **2013**, *7*, 4708.
(21) Dong, H.; Fu, X.; Liu, J.; Wang, Z.; Hu, W. *Adv. Mater.* **2013**, *25*, 6158.
(22) Graham, K. R.; Cabanetos, C.; Jahnke, J. P.; Idso, M. N.; Labban, A. L.; Ndjawa, G. O. N.; Heumueller, T.; Vandewal, K.; Salleo, A.; Chmelka, B. F.; Amassian, A.; Beaujuge, P. M.; McGehee, M. D. *J. Am. Chem. Soc.* **2014**, *136*, 9608.
(23) (a) Yuan, Q.; Mannsfeld, S. C. B.; Tang, M. L.; Toney, M. F.; Lüning, J.; Bao, Z. *J. Am. Chem. Soc.* **2008**, *130*, 3502. (b) Gann, E.; Gao, X.; Di, C.-a.; McNeill, C. R. *Adv. Funct. Mater.* **2014**, DOI: 10.1002/adfm.201401228.
(24) (a) Jackson, N. E.; Savoie, B. M.; Kohlstedt, K. L.; Marks, T. J.; Chen, L. X.; Ratner, M. A. *Macromolecules* **2014**, *47*, 987. (b) Perez, L. A.; Zalar, P.; Ying, L.; Schmidt, K.; Toney, M. F.; Nguyen, T.-Q.; Bazan, G. C.; Kramer, E. J. *Macromolecules* **2014**, *47*, 1403. (c) Ying, L.; Hsu, B. B. Y.; Zhan, H.; Welch, G. C.; Zalar, P.; Perez, L. A.; Kramer, E. J.; Nguyen, T.-Q.; Heeger, A. J.; Wong, W.-Y.; Bazan, G. C. *J. Am. Chem. Soc.* **2011**, *133*, 18538.
(25) Gao, X.; Hu, Y. *J. Mater. Chem. C* **2014**, *2*, 3099.
(26) Najari, A.; Beaupré, S.; Berrouard, P.; Zou, Y.; Pouliot, J.-R.; Lepage-Pérusse, C.; Leclerc, M. *Adv. Funct. Mater.* **2011**, *21*, 718.
(27) Kirby, N. M.; Mudie, S. T.; Hawley, A. M.; Cookson, D. J.; Mertens, H. D. T.; Cowieson, N.; Samardzic-Boban, V. *J. Appl. Crystallogr.* **2013**, *46*, 1670.